processes

MDPI

Article

Effects of Ti/Al Ratio on Formation of Ti-Al Intermetallics/TiB_2 Composites by SHS from Ti-Al-B Powder Mixtures

Chun-Liang Yeh * and Yi-Cheng Chan

Department of Aerospace and Systems Engineering, Feng Chia University, Taichung 407102, Taiwan
* Correspondence: clyeh@fcu.edu.tw; Tel.: +88-64-2451-7250 (ext. 3963)

Abstract: Ti-Al intermetallics/TiB_2 composites were prepared from elemental powder mixtures by the method of self-propagating high-temperature synthesis (SHS). Reactant mixtures were formulated to contain two parts; one group was (2Ti + 4B) to form $2TiB_2$ and the other group was (Ti + xAl) to produce Ti-Al intermetallic compounds. The content of Al ranged between x = 0.33 and 3.0, which was equivalent to the Ti/Al atomic ratio from Ti-25% Al to Ti-75% Al in the (Ti + xAl) group. The results showed that the increase of Al percentage reduced the overall combustion exothermicity and led to a slower self-sustaining combustion wave speed and a lower combustion temperature. Apparent activation energy of the Ti-Al-B solid-state combustion reaction was determined to be 114.7 kJ/mol by this study. Based on the XRD analysis, Ti-Al intermetallics/TiB_2 composites featuring Ti_3Al, TiAl, $TiAl_2$, and $TiAl_3$ as the dominant aluminide phase were respectively synthesized from the samples of Ti-25%~40% Al, Ti-50%~60% Al, Ti-71.4% Al, and Ti-75% Al. For the samples of Ti-25% Al and Ti-30% Al, Ti_3Al was the only aluminide formed. The microstructure of the composites exhibited that TiB_2 grains with a columnar shape of 2–3 μm in length were well distributed and embedded in the aluminide matrix. This study demonstrated an effective and energy-saving fabrication route for producing Ti-Al intermetallics/TiB_2 composites with different dominant aluminide phases.

Keywords: Ti-Al intermetallics; TiB_2; combustion synthesis; XRD; activation energy

check for updates

Citation: Yeh, C.-L.; Chan, Y.-C. Effects of Ti/Al Ratio on Formation of Ti-Al Intermetallics/TiB_2 Composites by SHS from Ti-Al-B Powder Mixtures. *Processes* **2024**, *12*, 1237. https://doi.org/10.3390/pr12061237

Academic Editor: Andrea Petrella

Received: 24 April 2024
Revised: 14 June 2024
Accepted: 15 June 2024
Published: 16 June 2024

Copyright: © 2024 by the authors. Licensee MDPI, Basel, Switzerland. This article is an open access article distributed under the terms and conditions of the Creative Commons Attribution (CC BY) license (https://creativecommons.org/licenses/by/4.0/).

1. Introduction

Titanium aluminide-based alloys and composites have attracted much attention for high-temperature structural applications in the automotive, aerospace, and nuclear industries [1,2]. Ti-Al intermetallics possess many unique properties, such as low density, high strength, excellent oxidation resistance, and creep resistance at elevated temperatures [1–3]. Alloying additions of 1–3 at.% of Cr, Nb, Ta, Mn, V, Mo, and Zr led to an increase in the low-temperature ductility and high-temperature strength as well as oxidation resistance of the Ti-Al intermetallics [3,4]. Formation of TiAl-based composites by adding ceramic particles has been shown to improve the mechanical and tribological properties of the Ti-Al intermetallics [5]. Ceramic compounds, for example TiB_2, Al_2O_3, B_4C, SiC, Ti_5Si_3, and Ti_2AlC, are thermally and chemically stable with the Ti-Al matrix and have been considered as the effective reinforcements [6–15]. Among most of the ceramic reinforcements, the coefficient of thermal expansion (CTE) of TiB_2 is similar to that of γ-TiAl alloys. Moreover, TiB_2 possesses high elastic modulus and outstanding wear resistance, and shows equal density to, and excellent chemical compatibility with, γ-TiAl alloys [6]. Fine TiB_2 particles with special morphology and induced bridging effect contributed to the notable fracture toughness of the TiAl/TiB_2 composite [7,8]. Therefore, in situ TiB_2 particles were found to significantly enhance the strength of TiAl alloys and have been adopted as a promising reinforcement for γ-TiAl based composites. For the TiB_2/TiAl composites prepared by the method of hot isostatic pressing, Li et al. [7] confirmed the strengthening effect of TiB_2 particulates and obtained the tensile stress of 653.4 ± 39.2 MPa and strain of 2.1 ± 0.33% for the TiB_2/TiAl composites. Han et al. [8] fabricated TiB_2-strengthened TiAl-based alloys by

the induction melting method and reported that such composites at 700 °C showed fracture toughness (K_{IC}) of 21.89 ± 0.84 MPa $m^{1/2}$, ultimate tensile strength (UTS) of 545 ± 19 MPa, and elongation-to-failure (ε_f) of 3.9% ± 0.18.

TiAl-based composites composed of in situ TiB_2 particles and 3 at.% Cr were prepared by hot pressing (HP) sintering from mixed Ti, Al, B, and Cr powders at 10 MPa and 1300 °C, and composites with a significant improvement in the yield strength and compressive strength were attained [6]. Li et al. [7] fabricated TiAl/TiB_2 composites alloyed with Nb, Cr, and C by hot isostatic pressing (HIP) at 1150 °C and 120 MPa for 3 h and showed that the tensile strength and strain of the composites increased with TiB_2 content. Lazurenko et al. [9] utilized spark plasma sintering (SPS) with Ti and Al foils and TiB_2 and TiC particles as the starting materials at 1250 °C to produce Ti_3Al/TiAl matrix composites reinforced by TiB_2 and Ti_2AlC. The composites displayed an improved compressive strength and better creep resistance [8]. With the use of the HP method operating at 1280 °C and 30 MPa for 2 h, a TiAl/Ti_3Al/Al_2O_3 composite was produced from pre-alloyed Ti, Al, Nb_2O_5, Nb, and B powder mixture [10]. In situ synthesis of a TiAl/Al_2O_3 composite from Ti, Al, Nb, W, and TiO_2 mixture was conducted by mechanical milling with subsequent spark plasma sintering [11]. Tan et al. [12] prepared Ti_3Al/TiAl composites with added SiC fibers by vacuum arc melting. The addition of SiC led to the formation of Ti_5Si_3 and Ti_2AlC, both of which contributed to better strength and ductility of the products [12]. Wang et al. [13] fabricated Ti_2AlC/TiAl composites with excellent room-temperature compression strength and fracture strain by the SPS technique using pre-alloyed Ti-48Al-2Cr-2Nb powders and graphene nanosheets as raw materials and operating at different temperatures of 1200–1320 °C for 10 min. TiAl/Ti_5Si_3 composites characterized by superplastic deformation were produced by high-energy ball milling of Ti, Al, and Si powders, followed by HIP at 1050–1150 °C and 300 MPa for 2 h [14]. Shu et al. [15] synthesized TiB_2- and Ti_5Si_3-reinforced TiAl composites from elemental powder blends by the thermal explosion method. TiB_2 particles were found to enhance the ultimate compression strength and Ti_5Si_3 particles to increase the strength and ductility of the composite [15]. Through combustion synthesis in the mode of self-propagating high-temperature synthesis (SHS), Yeh and Li [16] studied the formation of TiAl/Ti_5Si_3 and TiAl/Al_2O_3 composites. From elemental powder compacts, TiAl/Ti_5Si_3 composites were produced and the increase of the Ti_5Si_3 content facilitated sustainability of a steady combustion process. TiAl/Al_2O_3 composites were prepared from Ti, Al, and TiO_2 powders by the SHS process involving a thermite reaction in which TiO_2 was reduced by Al. The increase of Al_2O_3 lowered combustion exothermicity and was responsible for combustion wave propagation in a pulsating mode [16].

Of various fabrication methods, the SHS technique takes advantage of the highly exothermic reaction and is an energy-efficient, time-saving, facile, and low-cost approach. Moreover, the SHS method is an in situ fabrication route for preparation of composite materials [16,17]. The objective of this study was to investigate in situ formation of Ti-Al intermetallics/TiB_2 composites by the SHS process from elemental powder mixtures consisting of Ti, Al, and boron. According to the Ti-Al phase diagram [18–20], Ti-Al intermetallic compounds include α_2-Ti_3Al, γ-TiAl, $TiAl_2$, and $TiAl_3$. Ti_3Al has a wide homogeneity range from 22 at.% Al to approximately 35 at.% Al. Depending on temperature, the TiAl phase has a composition of 49–66 at.% Al. Two-phase alloys (γ-TiAl + α_2-Ti_3Al) exist between 35 at.% and 49 at.% Al. For the Al-rich compounds, $TiAl_2$ has a narrow homogeneity range of 64.5–67 at.% Al and $TiAl_3$ is a line compound. In this study, the effects on the combustion wave temperature and velocity of the Ti/Al atomic ratio from Ti-25 at.% Al to Ti-75 at.% Al were explored, as well as those on the Ti-Al intermetallic phases formed in the composite. Unlike most of the previous studies focusing only on the γ-TiAl phase, this work represents the first attempt to investigate the formation of Ti-Al intermetallics/TiB_2 composites featuring four different dominant aluminide phases. The activation energy of solid-state combustion of the Ti-Al-B system was deduced from combustion kinetics. Microstructure and composition of the synthesized composites were examined.

2. Materials and Methods

The materials used in this study included Ti (Alfa Aesar, Ward Hill, MA, USA, <45 μm, 99.8%), Al (Alfa Aesar, <45 μm, 99.8%), and amorphous boron (B) (Noah Technologies, San Antonio, TX, USA, < 1 μm, 93.5%). Reactant mixtures were formulated as in Equation (1):

$$(2\mathrm{Ti} + 4\mathrm{B}) + (\mathrm{Ti} + \mathrm{xAl}) \rightarrow 2\mathrm{TiB_2} + (\mathrm{Ti_3Al}, \mathrm{TiAl}, \mathrm{TiAl_2}, \mathrm{and/or} \mathrm{TiAl_3}) \quad (1)$$

As expressed in Equation (1), the amount of Ti in the reactant blend was divided into two groups. One part of Ti is to react with boron (i.e., 2Ti + 4B) to produce TiB_2, which is a highly exothermic phase. The other part of Ti is to react with Al to produce Ti-Al intermetallic compounds. The phase of titanium aluminide depends on the content of Al in the (Ti + xAl) group. As shown in Table 1, the parameter x varies from 0.33 to 3.0, which corresponds to the Ti/Al atomic ratio from Ti-25 at.% Al to Ti-75 at.% Al. The expression of Ti-25% Al means that the atomic percentage of Al in the (Ti + xAl) group with x = 0.33 is 25%. Likewise, Ti-75% Al represents 75% of Al in the (Ti + xAl) group for the case of x = 3.0. This type of expression for the Ti/Al atomic ratio was used in the following text. Based on stoichiometric balance under different values of x, Table 1 lists either sole or mixed Ti-Al intermetallic compounds to be formed as the products. It should be noted that the sample of x = 0.43 (Ti-30% Al) is an Al-rich condition to produce Ti_3Al, because Ti_3Al exists in a wide homogeneity range from 22 to 35 at.% Al.

Table 1. Ti/Al atomic ratio and Ti-Al intermetallics of Equation (1) under different values of x.

x	Ti/Al Atomic Ratio	Ti-Al Intermetallics
0.33	Ti-25% Al	1/3 Ti_3Al
0.43	Ti-30% Al	1/3 Ti_3Al
0.67	Ti-40% Al	1/6 Ti_3Al + 1/2 TiAl
1.0	Ti-50% Al	TiAl
1.5	Ti-60% Al	1/2 TiAl + 1/2 $TiAl_2$
2.0	Ti-66.7% Al	$TiAl_2$
2.5	Ti-71.4% Al	1/2 $TiAl_2$ + 1/2 $TiAl_3$
3.0	Ti-75% Al	$TiAl_3$

The combustion exothermicity of Equation (1) was evaluated by calculating the enthalpy of reaction (ΔH_r) at 298 K and adiabatic combustion temperature (T_{ad}) based on the intermetallic compositions presented in Table 1. Equation (2) is an energy balance equation for computing T_{ad} [21]. ΔH_r was calculated from the heats of formation (ΔH_f) of the reactants and products. The required thermochemical data including ΔH_f and heat capacity $c_p(P_i)$ of the product species are listed in Table 2 [22].

$$\Delta H_r + \int_{298}^{T_{ad}} \sum n_j c_p(P_j) dT + \sum_{298-T_{ad}} n_j L(P_j) = 0 \quad (2)$$

where n_j is the stoichiometric coefficient of the product and $L(P_j)$ is the latent heat of the product.

Table 2. Heat of formation (ΔH_f) and specific heat (c_p) of product species.

Product Species	Heat of Formation ΔH_f (kJ/mol)	Specific Heat, c_p (J/mol·K)
TiB_2	–315.9	$56.38 + 25.86 \cdot 10^{-3} \cdot T - 1.75 \cdot 10^{6} \cdot T^{-2}$
Ti_3Al	–97.9	$103.3 + 15.90 \cdot 10^{-3} \cdot T - 1.73 \cdot 10^{6} \cdot T^{-2}$
TiAl	–75.3	$49.2 + 8.85 \cdot 10^{-3} \cdot T - 0.75 \cdot 10^{6} \cdot T^{-2}$
$TiAl_2$	–90.4	$62.2 + 10.33 \cdot 10^{-3} \cdot T - 0.96 \cdot 10^{6} \cdot T^{-2}$
$TiAl_3$	–146.4	$98.9 + 19.34 \cdot 10^{-3} \cdot T - 1.66 \cdot 10^{6} \cdot T^{-2}$

The SHS experiments were performed in a windowed combustion chamber. The chamber was first purged with high-purity (99.99%) argon for 3 min and then filled with argon at 2 bars. Well-mixed powders were uniaxially compressed to form cylindrical test samples with a diameter of 7 mm, a height of 12 mm, and a relative density of 55%. The ignition of the powder compact was achieved by a heated tungsten coil with a voltage of 120 V and a current of 5 A. Based on the time series of recorded combustion images, the propagation velocity of the self-sustaining combustion wave (V_f) was determined from the time derivative of the combustion front trajectory. The exposure time of each recorded image was set at 0.1 ms. A beam splitter with a mirror characteristic of 75% transmission and 25% reflection was used to optically superimpose a scale onto the image of the sample in order to accurately measure the instantaneous locations of the combustion front. The combustion temperature was measured by a bare Pt/Pt-13%Rh (R-type) thermocouple with a bead diameter of 125 μm and the thermocouple was mounted at a position about 6–7 mm from the ignited top plane of the sample. Details of the experimental setup and approaches are presented elsewhere [23]. For the synthesized products, the phase composition was identified by a Bruker D2 X-ray diffractometer (XRD Phaser, Karlsruhe, Germany). Microstructure and elemental analysis of the final products were examined by scanning electron microscopy (Hitachi S-3400N, Tokyo, Japan) and energy-dispersive X-ray spectroscopy.

3. Results and Discussion

3.1. Analysis of Combustion Exothermicity

Variations in ΔH_r and T_{ad} of the test samples containing different amounts of Al in the (Ti + xAl) group of Equation (1) are presented in Figure 1. The reaction of Equation (1) is exothermic and the enthalpy of reaction increases from 664.4 to 778.2 kJ with an increase in Al percentage from 25% to 75%. Because TiB_2 and four different Ti-Al compounds were formed as exothermic phases, the increase of the total number of mole of Ti-Al intermetallic compounds produced in the composites was responsible for the increase of ΔH_r from Ti-25% Al to Ti-50% Al. For the samples containing more than Ti-50% Al, because an equal amount of Ti-Al compounds was produced, the increase of ΔH_r is ascribed to the formation of Al-rich phases, $TiAl_2$ and $TiAl_3$. As indicated in Table 2, the heat of formation between TiAl, $TiAl_2$, and $TiAl_3$ is in an ascending order.

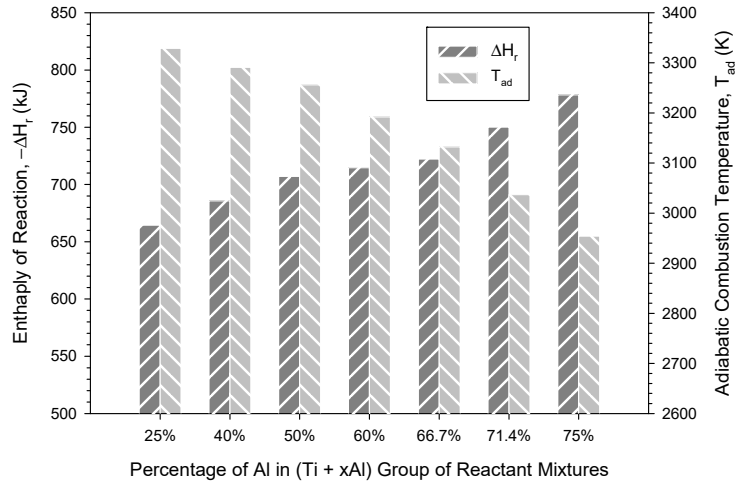


Figure 1. Variations of enthalpy of reaction (ΔH_r) and adiabatic combustion temperature (T_{ad}) with Al percentage in the (Ti + xAl) group of reactant mixtures.

In contrast, Figure 1 shows that the T_{ad} of Equation (1) decreased from 3329 to 2954 K with increasing Al content in the samples from Ti-25% Al to Ti-75% Al. The high adiabatic combustion temperatures provide sufficient exothermicity for a self-sustaining reaction. Based on the heat of formation and specific heat of each compound listed in Table 2,

TiB_2 was the most exothermic phase to form in the composite. Within Equation (1), the reaction of Ti with boron is considered as not only the major heat-releasing step but also the initiation step. Although the interaction of Ti with Al liberates heat in producing Ti-Al intermetallics, its exothermicity is less than the formation of TiB_2. As a result, the overall reaction exothermicity is weakened when the mole fraction of Ti-Al compounds augmented in the composite. This explains the descent of T_{ad} for the samples containing Al from Ti-25% Al to Ti-50% Al. Further decline in T_{ad} for the samples with Al percentage from Ti-50% Al to Ti-75% Al was mainly caused by the formation of Al-rich phases, $TiAl_2$ and $TiAl_3$, both of which have large specific heats.

3.2. Self-Propagating Combustion Wave Kinetics

Figure 2a–c illustrate typical time sequences of the SHS processes, which were respectively recorded from powder compacts formulated with Ti-25% Al, Ti-50% Al, and Ti-75% Al. It is evident that the combustion reaction started upon ignition and established a distinct combustion wave that propagated throughout the entire sample in a self-sustaining manner. Self-sustaining combustion was achieved for all samples conducted in this study. With the increase of Al percentage in the reactant mixture, as shown in Figure 2a–c, the burning luminosity decreased to some extent and the total spreading time of combustion wave was notably prolonged from about 1.50 s to 1.83 s and then to 3.97 s. These observations reflect the fact that combustion exothermicity decreased with increasing Al content in the reactant mixture.

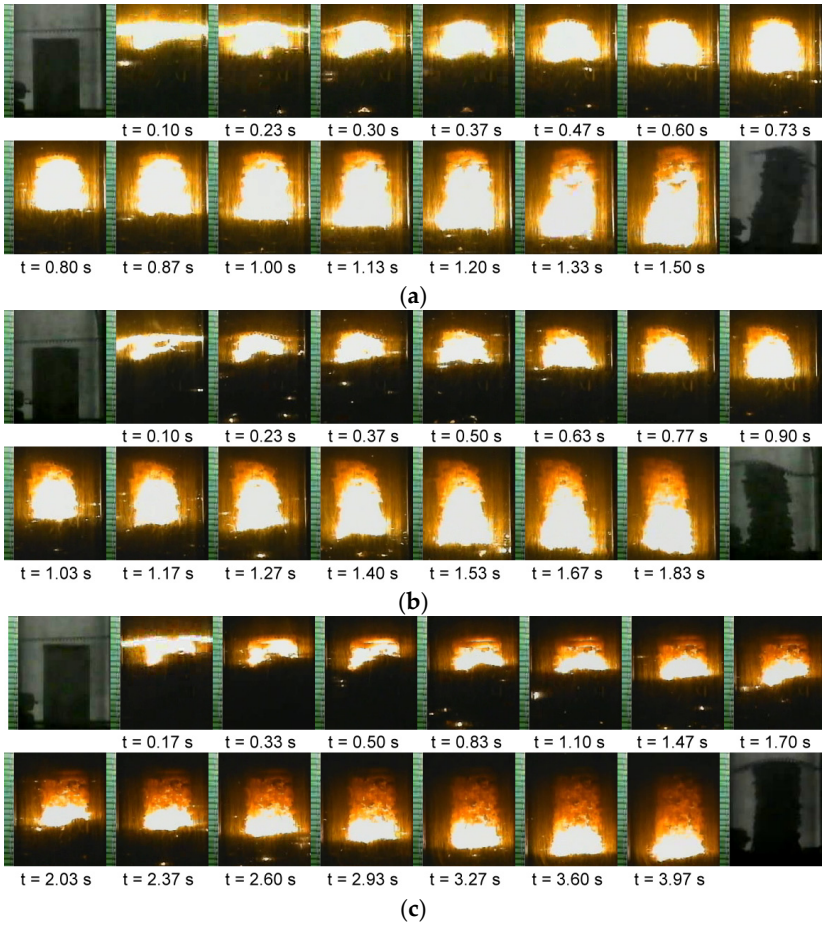


Figure 2. Series of self-sustaining combustion images recorded from powder compacts of Equation (1) with (**a**) Ti-25% Al, (**b**) Ti-50% Al, and (**c**) Ti-75% Al (unit of scale bar: 1 mm).

The variation of combustion front velocity (V_f) with Al percentage in the (Ti + xAl) group of the reactant mixture is presented in Figure 3. The velocity decreased moderately

from 6.6 to 5.6 mm/s as the Al content increased from Ti-20% Al to Ti-50% Al, beyond which a significant drop in combustion velocity was observed. The lowest flame velocity of about 2.2 mm/s was detected for the sample of Ti-75% Al. It is believed that energy transfer by heat conduction from the thin reaction zone to its adjacent unburned region is of critical importance to maintain a self-sustaining combustion process. As a result, the flame-front propagation velocity, in large part, is governed by the combustion wave temperature.

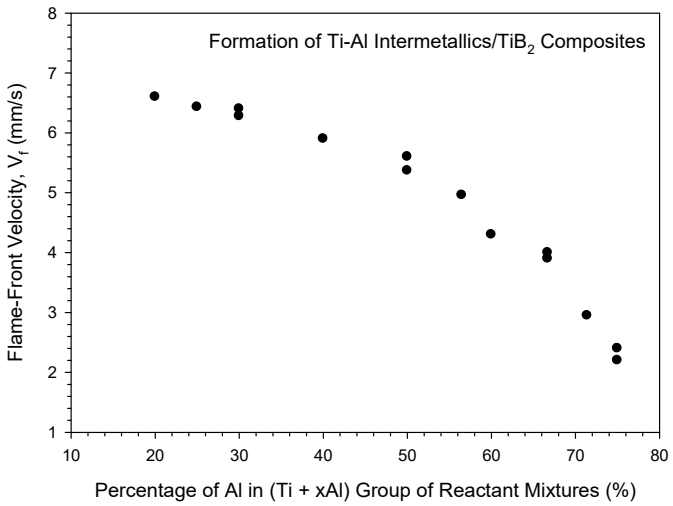


Figure 3. Variation of combustion wave propagation velocity with Al percentage in the (Ti + xAl) group of reactant mixtures.

Figure 4 depicts four combustion temperature profiles measured from the powder compacts formulated with different Al percentages. Temperature profiles featured a sharp rise to a peak value followed by a continuous decline. This could be caused by the fact that the combustion propagation was speedy and synthesis reaction was normally confined in a hot thin layer. Moreover, the product was formed and cooled down after the passage of the combustion front. The peak value is considered as the combustion front temperature (T_c). As revealed in Figure 4, T_c reached 1655 °C for the sample of Ti-25% Al and decreased to about 1574 °C and 1442 °C with an increase in Al content to Ti-50% Al and Ti-66.7% Al, respectively. The sample of Ti-75% Al exhibited a less steep curve with T_c of about 1278 °C. More importantly, the dependency of combustion temperature on sample stoichiometry was consistent with that of combustion wave velocity.

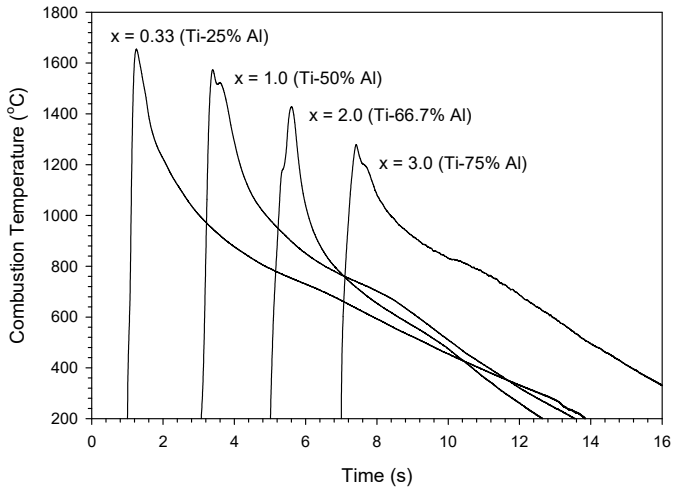


Figure 4. Combustion temperature profiles of compacted samples formulated with Ti-25% Al, Ti-50% Al, Ti-66.7% Al, and Ti-75% Al.

According to combustion wave kinetics [23,24], a modified Arrhenius rate equation, Equation (3), was employed to deduce the apparent activation energy (E_a) of solid-state combustion reaction.

$$V_f^2 = \frac{2\lambda}{\rho Q}\frac{RT_c^2}{E_a}k_o \exp(-E_a/RT_c) \quad (3)$$

where λ is the thermal conductivity, R is the universal gas constant, Q is the heat of the reaction, and k_o is a constant. Based on Equation (3), the relationship of $\ln(V_f/T_c)^2$ with $1/T_c$ can be established by the measured data of V_f and T_c, and the slope of a linear line correlating $\ln(V_f/T_c)^2$ and $1/T_c$ represents E_a/R. Figure 5 plots calculated values of $-\ln(V_f/T_c)^2$ with respect to $1/T_c$ and a best-fitted linear line with the slope. Activation energy E_a equal to 114.7 kJ/mol was deduced for the Ti-Al-B combustion reaction. This value is much lower than the activation energy, 539 kJ/mol, obtained in the Ti + 2B combustion reaction [25]. It is believed that due to the presence of liquid-phase Al during combustion synthesis, the activation energy of the ternary Ti-Al-B combustion system was reduced. Combustion temperatures of this study shown in Figure 4 are higher than the melting point of Al. The existence of molten species could have facilitated the diffusion of solid reactants and substantially reduced the kinetic barrier of the reaction system. A similar example confirming the aid of molten species is that the activation energy of 102.5 kJ/mol was determined for the Ti-B_4C-Al-Ni combustion system to produce NiAl/TiB_2/TiC composites [26].

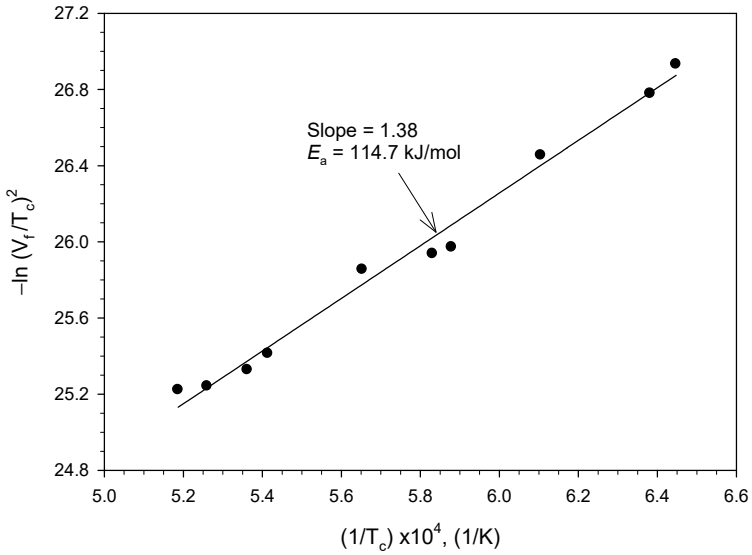


Figure 5. Linear correlation between $\ln(V_f/T_c)^2$ and $1/T_c$ and activation energy (E_a) of the Ti-Al-B combustion reaction.

3.3. Phase Composition and Microstructure of Synthesized Products

Figure 6a–d present XRD patterns of Ti-Al intermetallics/TiB_2 composites synthesized from powder compacts with different Al percentages in the (Ti + xAl) group of reactant mixtures. The other mixture group in Equation (1) generated TiB_2. The XRD analysis revealed that TiB_2 was well produced from the elemental reaction between Ti and boron for all samples and the phase of the intermetallic compound was subject to the Al percentage in the (Ti + xAl) group. The sample of Ti-30% Al, shown in Figure 6a, produced only Ti_3Al, which was also the only aluminide produced from the sample of Ti-25% Al. This agrees with the fact that Ti_3Al has a wide homogeneity range from 22 to 35 at.% Al.

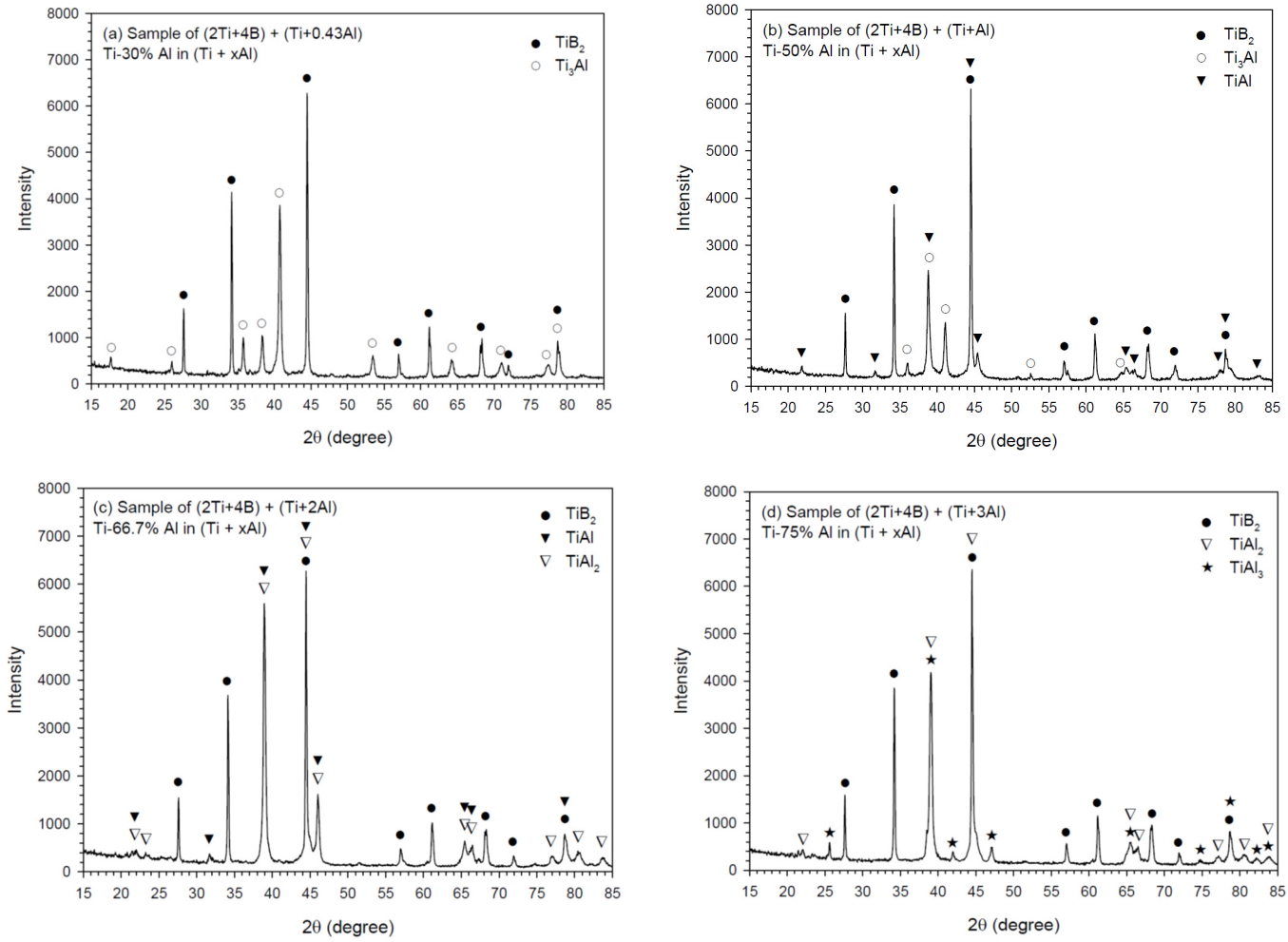


Figure 6. XRD patterns of Ti-Al intermetallics/TiB_2 composites synthesized from the samples containing different percentages of Al in the (Ti + xAl) group of reactant mixtures: (**a**) Ti-30% Al, (**b**) Ti-50% Al, (**c**) Ti-66.7% Al, and (**d**) Ti-75% Al.

Figure 6b depicts the XRD spectrum of the product synthesized from the sample of Ti-50% Al. Formation of TiB_2 along with two aluminides, TiAl and Ti_3Al, was identified. The dominant intermetallic phase in Figure 6b is TiAl. The presence of Ti_3Al could be due to the evaporation loss of a small amount of Al during the SHS process, or because of TiAl having a composition range from 49 at.% Al to about 66 at.% Al. Both TiAl and Ti_3Al were also formed in the product from the sample with Ti-40% Al, which was consistent with the coexistence of TiAl and Ti_3Al in the composition between Ti-35 at.% Al and Ti-49 at.% Al. However, the governing aluminide phase was Ti_3Al in the product of Ti-40% Al.

The product composed of TiB_2, TiAl, and $TiAl_2$, as displayed in Figure 6c, is associated with the sample of Ti-66.7% Al. Since $TiAl_2$ has a narrow homogeneity range of 64.5–67 at.% Al and TiAl has a Al-rich composition of about 60–66 at.% Al at temperatures between 1200 °C and 1400 °C, a small evaporation loss of Al could result in the formation of TiAl. It is useful to mention that the formation of TiAl was more pronounced in the product from the sample of Ti-60% Al than that revealed in Figure 6c. Namely, TiAl dominated over $TiAl_2$ in the TiAl/$TiAl_2$/TiB_2 composite synthesized from the sample of Ti-60% Al, while TiAl and $TiAl_2$ were nearly comparable in the product from the sample of Ti-66.7% Al.

The XRD pattern of Figure 6d represents the product obtained from the sample of Ti-75% Al. The yield of $TiAl_3$ as the major aluminide is identified. The presence of a small amount of $TiAl_2$ in the product was because $TiAl_3$ is a line compound. Therefore, a slight deficiency of Al might lead to the formation of $TiAl_2$. It should be noted that a composite

consisting of TiB_2, $TiAl_2$, and $TiAl_3$ was also synthesized from the sample of Ti-71.4% Al and the content of $TiAl_2$ relative to $TiAl_3$ was more than that observed in Figure 6d. Table 3 summarizes the major and minor phases of titanium aluminides formed in the TiB_2-containing composites from combustion of Equation (1) under different contents of Al. It is evident that Ti-Al intermetallics/TiB_2 composites featuring four different dominant aluminide phases were produced.

Table 3. Major and minor titanium aluminides of Ti-Al intermetallics/TiB_2 composites synthesized from Equation (1) with different Al percentages in the (Ti + xAl) group.

Al Percentage in Ti + xAl	Major Aluminide	Minor Aluminide
Ti-25% Al	Ti_3Al	—
Ti-30% Al	Ti_3Al	—
Ti-40% Al	Ti_3Al	TiAl
Ti-50% Al	TiAl	Ti_3Al
Ti-60% Al	TiAl	$TiAl_2$
Ti-66.7% Al	$TiAl_2$, TiAl	—
Ti-71.4% Al	$TiAl_2$	$TiAl_3$
Ti-75% Al	$TiAl_3$	$TiAl_2$

Figure 7 presents the SEM image and EDS spectrum, showing fracture surface microstructure and elemental composition of the product synthesized from the sample of Ti-30% Al. Most of the TiB_2 grains were formed in a columnar shape with a length of 2–3 μm and were embedded in the Ti-Al aluminide matrix. According to the formation mechanism of Ti-Al intermetallics [3,27], the stages involve the initial melting of Al, subsequent spreading of molten Al through channels of the capillary-porous medium, and diffusion of aluminum atoms into the titanium lattice. This resulted in the formation of the $TiAl_3$ compound, which can transform into $TiAl_2$, TiAl, and Ti_3Al as it is saturated with titanium. The formation of TiB_2 is governed by a dissolution/precipitation mechanism including solid-phase diffusion of boron into titanium and the precipitation of TiB_2 particles [28,29]. The EDS spectrum of Figure 7 confirms three constituent elements, from which an atomic ratio of B:Al:Ti = 55.84:8.94:35.22 was obtained. Low Al proportion was ascribed to this composite containing a Ti-rich aluminide Ti_3Al at a small mole fraction.

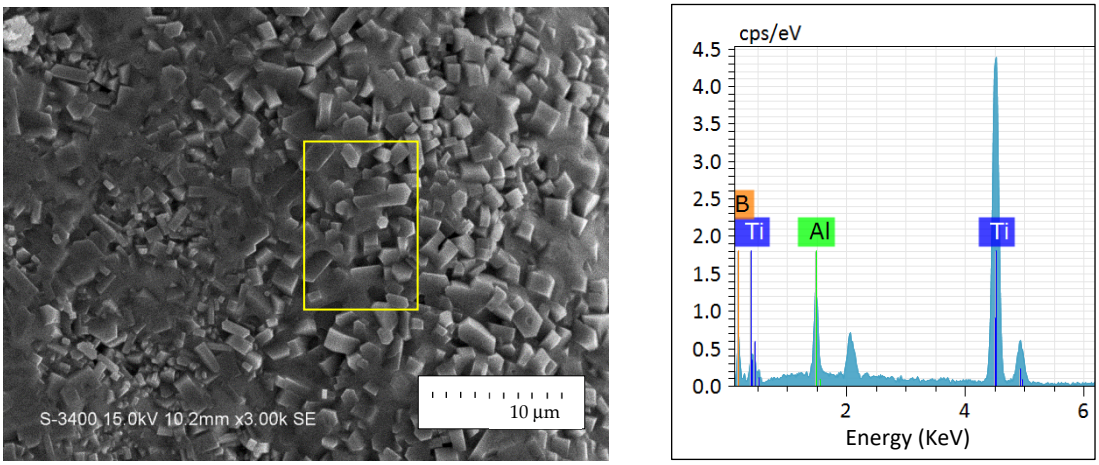


Figure 7. SEM micrograph and EDS spectrum of Ti_3Al/TiB_2 composite synthesized from the sample of Ti-30% Al.

The SEM image and EDS spectrum presented in Figure 8 are associated with the product obtained from the sample of Ti-50% Al. The morphology clearly exhibited columnar TiB_2 grains well distributed in the Ti-Al aluminide matrix. The EDS intensity of the Al

peak relative to that of Ti in Figure 8 is noticeably stronger than that observed in Figure 7. The atomic ratio of the scanned region was B:Al:Ti = 45.89:15.22:38.89, which is close to a composite consisting of TiB_2 and TiAl. It should be noted that the peak at around 2.1 keV is Pt (platinum). In this study, Pt was used to sputter coat SEM samples as a conductive layer.

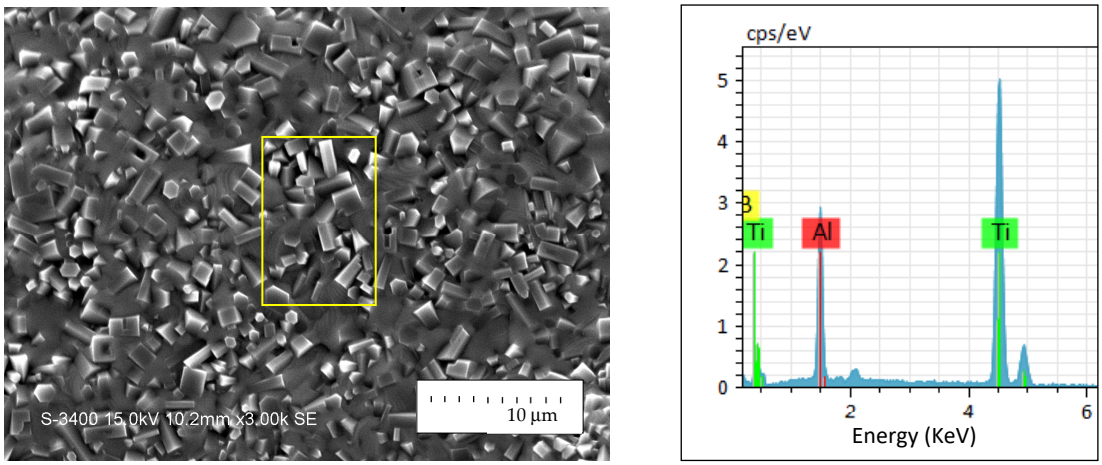


Figure 8. SEM micrograph and EDS spectrum of $TiAl/Ti_3Al/TiB_2$ composite synthesized from the sample of Ti-50% Al.

For the sample of Ti-75% Al, the microstructural and elemental analyses of its resulting product are unveiled in Figure 9. TiB_2 grains were formed in a smaller size of about 1 µm and mixed closely with the Ti-Al aluminide matrix. When compared with that in Figure 8, an Al peak with a further increase in intensity was detected in the EDS spectrum of Figure 9. An atomic ratio of B:Al:Ti = 40.54:28.64:30.82 was obtained, which suggested $TiAl_3$ as the dominant aluminide in the Ti-Al intermetallics/TiB_2 composite. It is important to note that the major titanium aluminide revealed by the atomic ratio of constituent elements from the EDS analysis of Figures 7–9 was in good agreement with the intermetallic phase identified by the XRD pattern.

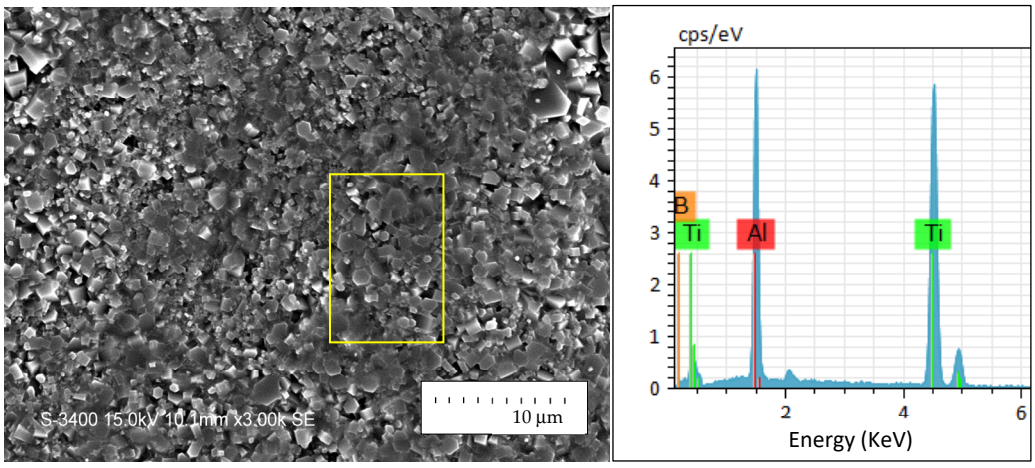


Figure 9. SEM micrograph and EDS spectrum of $TiAl_3/TiAl_2/TiB_2$ composite synthesized from the sample of Ti-75% Al.

The green powder compacts conducted by this work had a relative density of 55%. Due to volume expansion of the burned samples after the SHS process, the final products were porous and had an estimated porosity of about 50%. As a result, composite powders were easy to obtain. In view of practical applications, the size range and external morphology of

Ti-Al intermetallics/TiB_2 composite powders are suitable as feedstock materials for powder metallurgy or in different thermal spraying systems for depositing protective coatings.

4. Conclusions

In situ formation of Ti-Al intermetallics/TiB_2 composites was investigated by the SHS technique from Ti-Al-B powder mixtures. The reactant mixtures comprised Ti and boron in a configuration of (2Ti + 4B) to produce $2TiB_2$, as well as Ti and Al in a composition of (Ti + xAl) to generate titanium aluminide. The phase of aluminide compounds formed depended on the Al content in the (Ti + xAl) group. A value of x ranging from 0.33 to 3.0 was conducted, which corresponded to the Ti/Al atomic ratio from Ti-25% Al to Ti-75% Al for studying the formation of four different aluminides, Ti_3Al, TiAl, $TiAl_2$, and $TiAl_3$.

Combustion exothermicity of the reaction was sufficient to ensure progression of the synthesis process in the SHS manner. However, combustion exothermicity was weakened by an increasing Al percentage in the reactant mixture due to the increase of aluminide compounds formed and the high specific heats of Al-rich aluminide phases. As a result, the combustion wave velocity decreased from 6.6 to 2.2 mm/s and combustion temperature from 1655 °C to 1278 °C when the Al percentage in the sample increased from Ti-25% Al to Ti-75% Al. Based on combustion wave kinetics, the apparent activation energy of 114.7 kJ/mol was deduced for the Ti-Al-B combustion reaction. The XRD analysis of the final products indicated that Ti_3Al was the only intermetallic compound synthesized from samples of Ti-25% Al and Ti-30% Al. A composite containing TiB_2, Ti_3Al, and TiAl was produced from the sample of Ti-40% Al. TiAl was the dominant aluminide in the products from samples of Ti-50% Al and Ti-60% Al. For the samples with Ti-66.7% Al and Ti-75% Al, their resulting products were $TiAl_2$/TiAl/TiB_2 and $TiAl_3$/$TiAl_2$/TiB_2 composites, respectively. The transformation of the dominant aluminide from the Ti-rich to Al-rich phase was a consequence of the increase of Al in the samples, and the synthesized intermetallic compounds with respect to the Ti/Al ratio in the samples were essentially in good agreement with titanium aluminides in the Ti-Al phase diagram. The microstructure of the as-synthesized Ti-Al intermetallics/TiB_2 composites illustrated that columnar TiB_2 grains with a length of 2–3 μm were formed and well distributed and closely engaged in the aluminide matrix. The EDS analysis confirmed constituent elements and provided rational atomic ratios between Ti, Al, and B. In summary, this study demonstrated an effective synthesis route for fabricating Ti-Al intermetallics/TiB_2 composites featuring different dominant aluminide phases.

Author Contributions: Conceptualization, C.-L.Y.; validation, C.-L.Y. and Y.-C.C.; methodology, C.-L.Y. and Y.-C.C.; data curation, C.-L.Y. and Y.-C.C.; formal analysis, C.-L.Y. and Y.-C.C.; resources, C.-L.Y.; investigation, C.-L.Y. and Y.-C.C.; writing—original draft preparation, C.-L.Y. and Y.-C.C.; writing—review and editing, C.-L.Y. and Y.-C.C.; project administration, C.-L.Y.; supervision, C.-L.Y.; funding acquisition, C.-L.Y. All authors have read and agreed to the published version of the manuscript.

Funding: This research was funded by the National Science and Technology Council of Taiwan, and the grant number was NSTC 112-2221-E-035-041-MY2.

Data Availability Statement: The data presented in this study are available in the article.

Conflicts of Interest: The authors declare no conflicts of interest.

References

1. Genc, O.; Unal, R. Development of gamma titanium aluminide (γ-TiAl) alloys: A review. *J. Alloys Compd.* **2022**, *929*, 167262. [CrossRef]
2. Liu, P.; Xie, J.; Wang, A. Recent research progress in TiAl matrix composites: A review. *J. Mater. Sci.* **2022**, *57*, 16147–16174. [CrossRef]
3. Avdeeva, V.; Bazhina, A.; Antipov, M.; Stolin, A.; Bazhin, P. Relationship between structure and properties of intermetallic materials based on γ-TiAl hardened in situ with Ti_3Al. *Metals* **2023**, *13*, 1002. [CrossRef]

4. Musi, M.; Graf, G.; Clemens, H.; Spoerk-Erdely, P. Alloying elements in intermetallic γ-TiAl based alloys–a review on their influence on phase equilibria and phase transformations. *Adv. Eng. Mater.* **2023**, *26*, 2300610. [CrossRef]
5. Chen, Z.; Liu, J.; Wang, Y.; Ma, T.; Zhu, D.; Xing, Q.; Feng, H.; Chen, R. High-temperature oxidation behavior of ceramic particles-reinforced TiAl composites with multilayered structure. *Ceram. Int.* **2024**, *50*, 2233–2241. [CrossRef]
6. Wei, Y.; Qiu, F.; Shu, S.; Tong, H.; Yang, H.; Jiang, Q. Microstructure manipulation and strengthening mechanism of TiAl composites reinforced by Cr solid solution and in-situ nanometer-sized TiB_2 particles. *Mater. Sci. Eng. A* **2022**, *845*, 143214.
7. Li, W.; Yang, Y.; Li, M.; Liu, J.; Cai, D.; Wei, Q.; Yan, C.; Shi, Y. Enhanced mechanical property with refined microstructure of a novel γ-TiAl/TiB_2 metal matrix composite (MMC) processed via hot isostatic press. *Mater. Design* **2018**, *141*, 57–66. [CrossRef]
8. Han, J.; Xiao, S.; Tian, J.; Chen, Y.; Xu, L.; Wang, X.; Jia, Y.; Rahoma, H.K.S.; Du, Z.; Cao, S. Microstructure characterization, mechanical properties and toughening mechanism of TiB_2-containing conventional cast TiAl-based alloy. *Mater. Sci. Eng. A* **2015**, *645*, 8–19. [CrossRef]
9. Lazurenko, D.V.; Stark, A.; Esikov, M.A.; Paul, J.; Bataev, I.A.; Kashimbetova, A.A.; Mali, V.I.; Lorenz, U.; Pyczak, F. Ceramic-reinforced γ-TiAl-based composites: Synthesis, structure, and properties. *Materials* **2019**, *12*, 629. [CrossRef]
10. Lu, X.; Li, J.; Chen, X.; Qiu, J.; Wang, Y.; Liu, B.; Liu, Y.; Rashad, M.; Pan, F. Mechanical, tribological and electrochemical corrosion properties of in-situ synthesized Al_2O_3/TiAl composites. *Intermetallics* **2020**, *120*, 106758. [CrossRef]
11. Lu, X.; Li, J.; Chen, X.; Ran, C.; Wang, Y.; Liu, B.; Liu, Y.; Rashad, M.; Pan, F. Grinding mechanism and mechanical properties of the in-situ synthesized Al_2O_3/TiAl composites. *Ceram. Int.* **2019**, *45*, 12113–12121. [CrossRef]
12. Tan, Y.; Chen, R.; Fang, H.; Liu, Y.; Ding, H.; Su, Y.; Guo, J.; Fu, H. Microstructure evolution and mechanical properties of TiAl binary alloys added with SiC fibers. *Intermetallics* **2018**, *98*, 69–78. [CrossRef]
13. Wang, Z.; Liu, P.; Wang, A.; Xie, J.; Hou, B. Effect of spark plasma sintering temperature on the multi-scale microstructure evolution and mechanical properties of Ti_2AlC/TiAl composites with network architecture. *J. Mater. Res. Technol.* **2023**, *25*, 6209–6223. [CrossRef]
14. Suryanarayana, C.; Behn, R.; Klassen, T.; Bormann, R. Mechanical characterization of mechanically alloyed ultrafine-grained Ti_5Si_3+ 40 vol% γ-TiAl composites. *Mater. Sci. Eng. A* **2013**, *579*, 18–25. [CrossRef]
15. Shu, S.; Xing, B.; Qiu, F.; Jin, S.; Jiang, Q. Comparative study of the compression properties of TiAl matrix composites reinforced with nano-TiB_2 and nano-Ti_5Si_3 particles. *Mater. Sci. Eng. A* **2013**, *560*, 596–600. [CrossRef]
16. Yeh, C.L.; Li, R.F. Formation of TiAl–Ti_5Si_3 and TiAl–Al_2O_3 in situ composites by combustion synthesis. *Intermetallics* **2008**, *16*, 64–70. [CrossRef]
17. Levashov, E.A.; Mukasyan, A.S.; Rogachev, A.S.; Shtansky, D.V. Self-propagating high-temperature synthesis of advanced materials and coatings. *Int. Mater. Rev.* **2017**, *62*, 203–239. [CrossRef]
18. Cobbinah, P.V.; Matizamhuka, W.R. Solid-state processing route, mechanical behaviour, and oxidation resistance of TiAl alloys. *Adv. Mater. Sci. Eng.* **2019**, *2019*, 1–21. [CrossRef]
19. Lei, C.; Xu, Q.; Sun, Y.Q. Phase orientation relationships in the TiAl–$TiAl_2$ region. *Mater. Sci. Eng. A* **2001**, *313*, 227–236. [CrossRef]
20. Peng, M.; Shou, H.; Cao, Y. First-principles calculations of structural, elastic and thermodynamic properties of (h, r)-$TiAl_2$. *Phys. B Condens. Matter* **2019**, *561*, 29–36. [CrossRef]
21. Zaki, Z.I.; Ahmed, Y.M.Z.; Abdel-Gawad, S.R. In-situ synthesis of porous magnesia spinel/TiB_2 composite by combustion technique. *J. Ceram. Soc. Jpn.* **2009**, *117*, 719–723. [CrossRef]
22. Binnewies, M.; Milke, E. *Thermochemical Data of Elements and Compounds*; Wiley-VCH Verlag GmbH: Weinheim, Germany, 2002.
23. Yeh, C.L.; Chen, C. In situ formation of titanium diboride/magnesium titanate composites by magnesiothermic-based combustion synthesis. *Processes* **2024**, *12*, 459. [CrossRef]
24. Varma, A.; Rogachev, A.S.; Mukasyan, A.S.; Hwang, S. Combustion synthesis of advanced materials: Principals and applications. *Adv. Chem. Eng.* **1998**, *24*, 79–225.
25. Holt, J.B.; Kingman, D.D.; Bianchini, G.M. Kinetics of the combustion synthesis of TiB_2. *Mater. Sci. Eng.* **1985**, *71*, 321–327. [CrossRef]
26. Yeh, C.L.; Ke, C.Y.; Chen, Y.C. In situ formation of TiB_2/TiC and TiB_2/TiN reinforced NiAl by self-propagating combustion synthesis. *Vacuum* **2018**, *151*, 185–188. [CrossRef]
27. Kurbatkina, V.V. Titanium Aluminides. In *Concise Encyclopedia of Self-Propagating High-Temperature Synthesis*; Borovinskaya, I.P., Gromov, A.A., Levashov, E.A., Maksimov, Y.M., Mukasyan, A.S., Rogachev, A.S., Eds.; Elsevier: Amsterdam, The Netherlands, 2017; pp. 392–393.
28. Shen, P.; Zou, B.; Jin, S.; Jiang, Q. Reaction mechanism in self-propagating high temperature synthesis of TiC-TiB_2/Al composites from an Al-Ti-B_4C system. *Mater. Sci. Eng. A* **2007**, *454*, 300–309. [CrossRef]
29. Fjellstedt, J.; Jarfors, A.E. On the precipitation of TiB_2 in aluminum melts from the reaction with KBF_4 and K_2TiF_6. *Mater. Sci. Eng. A* **2005**, *413*, 527–532. [CrossRef]

Disclaimer/Publisher's Note: The statements, opinions and data contained in all publications are solely those of the individual author(s) and contributor(s) and not of MDPI and/or the editor(s). MDPI and/or the editor(s) disclaim responsibility for any injury to people or property resulting from any ideas, methods, instructions or products referred to in the content.